Science Advances
AAAS

advances.sciencemag.org/cgi/content/full/5/5/eaaw5558/DC1

Supplementary Materials for

Ultrafast correlated charge and lattice motion in a hybrid metal halide perovskite

Yang Lan, Benjamin J. Dringoli, David A. Valverde-Chávez, Carlito S. Ponseca Jr., Mark Sutton, Yihui He, Mercouri G. Kanatzidis, David G. Cooke*

*Corresponding author. Email: cooke@physics.mcgill.ca

Published 31 May 2019, *Sci. Adv.* **5**, eaaw5558 (2019)
DOI: 10.1126/sciadv.aaw5558

This PDF file includes:

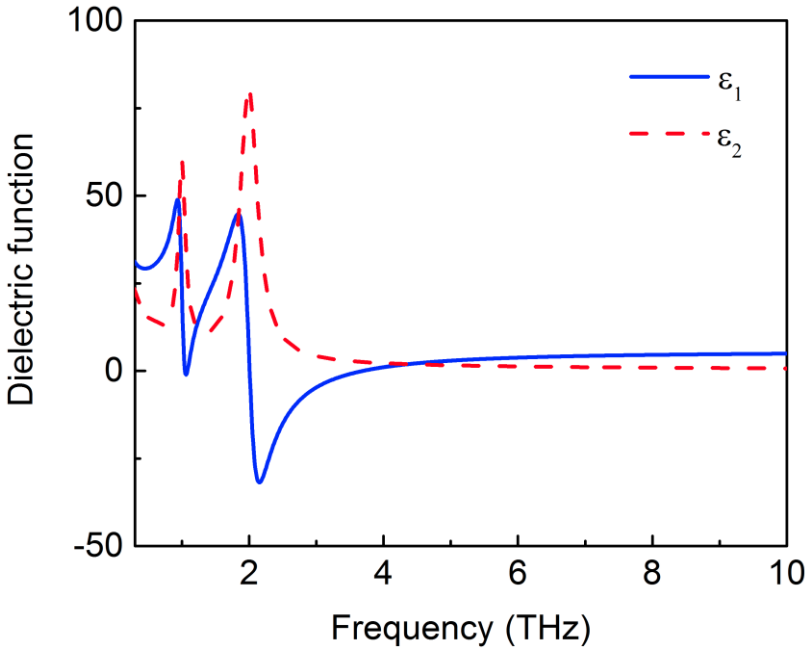

Fig. S1. Static dielectric function of MAPI. Real part (blue solid line) and imaginary part (red dash line) of MAPI dielectric function from the model in Ref (*31*).

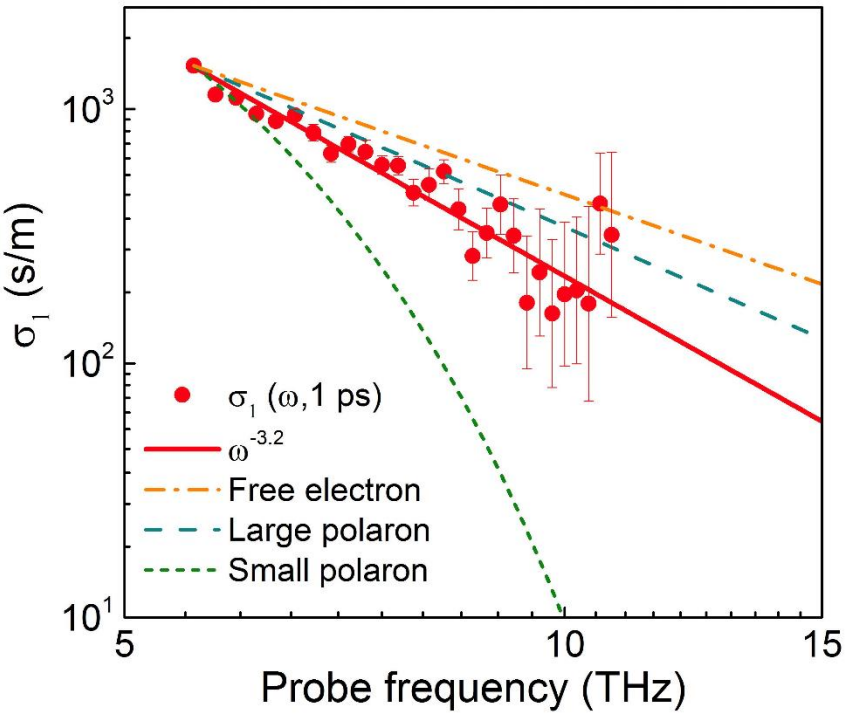

Fig. S2. Conductivity of MAPI at τ =1 ps. Real part of high frequency conductivity (red dots) with error bars representing standard deviation by THz reflection measurement at ⟨111⟩ facet, the power law fitting (solid line) with $\omega^{-3.2\pm0.2}$, the free electron case (dash dots) with ω^{-2}, the large polaron limit (dash line) with $\omega^{-2.5}$, and the small polaron limit (short dash line) with a Gaussian shape rolling down.

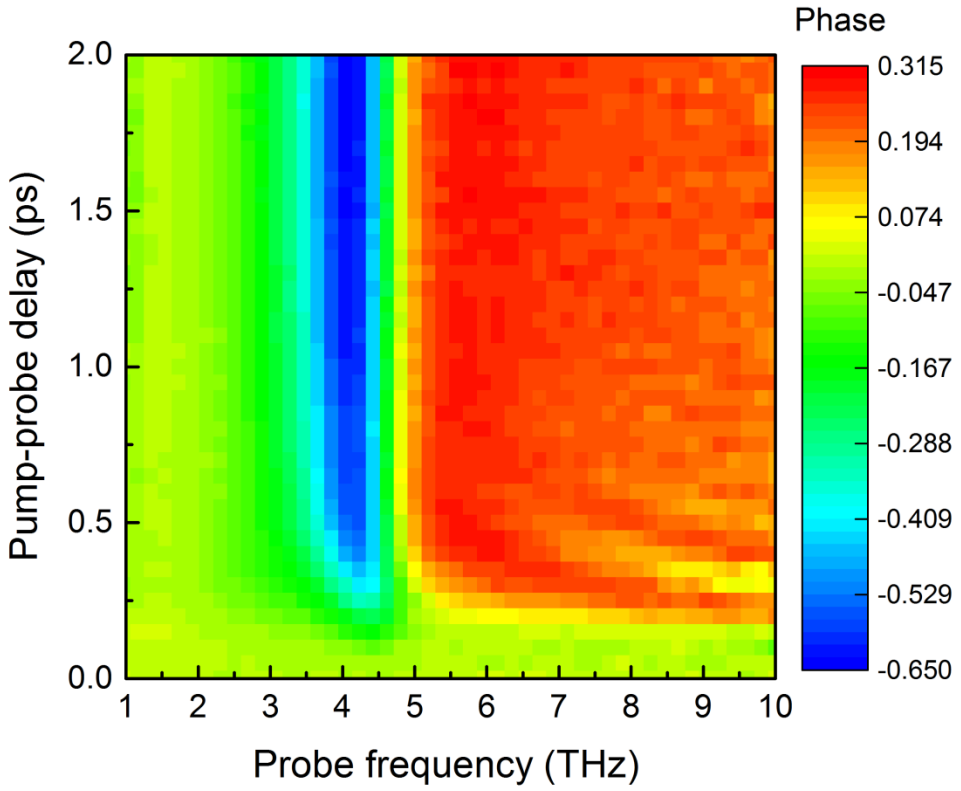

Fig. S3. Phase of pump-induced differential THz reflectivity at the $\langle 11\bar{1} \rangle$ facet. Two-dimensional pump-probe delay time/probe frequency map of phase for $\boldsymbol{\Delta r(\omega, \tau)/r_0}$ at the $\langle 11\bar{1} \rangle$ facet.

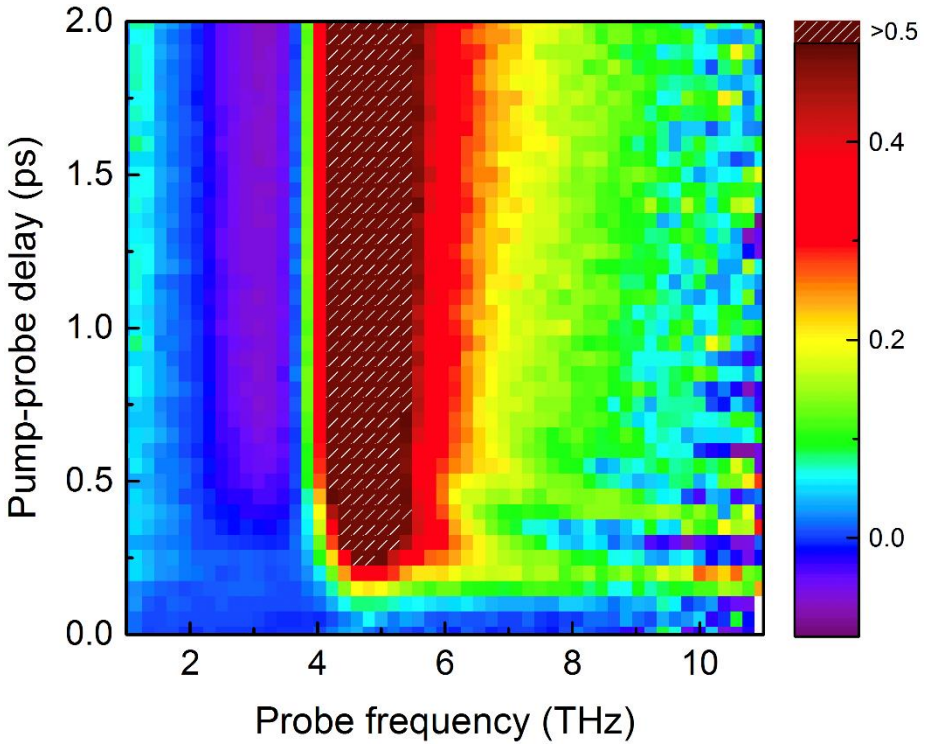

Fig. S4. Amplitude of pump-induced differential THz reflectivity at the ⟨100⟩ facet. Two-dimensional pump-probe delay time/probe frequency map of phase for $\boldsymbol{\Delta r(\omega,\tau)/r_0}$ at the ⟨10**0**⟩ facet under the same TRTS measurement at the ⟨10**0**⟩ facet.

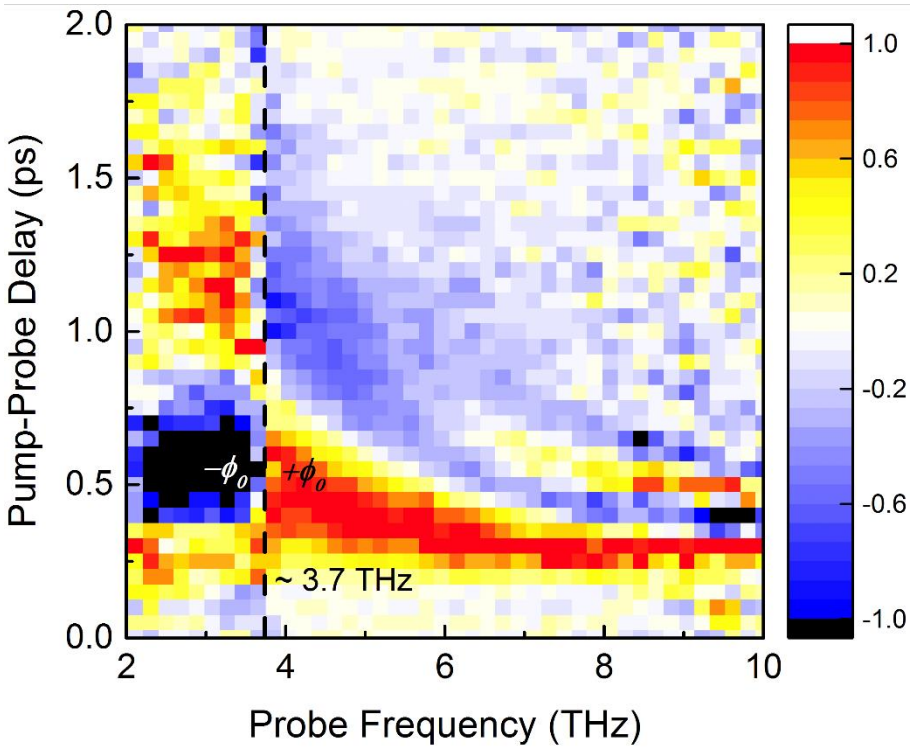

Fig. S5. Time domain coherent oscillations of THz reflectivity without slow rise component at ⟨100⟩ facet. Normalized $|\Delta r(\omega,\tau)|_{osc}^{norm}$ map with slow rise component subtracted. The vertical dash line marks the LO phonon frequency at 3.7 THz where a π phase flip occurs and above which a subsequent frequency chirp is evident.

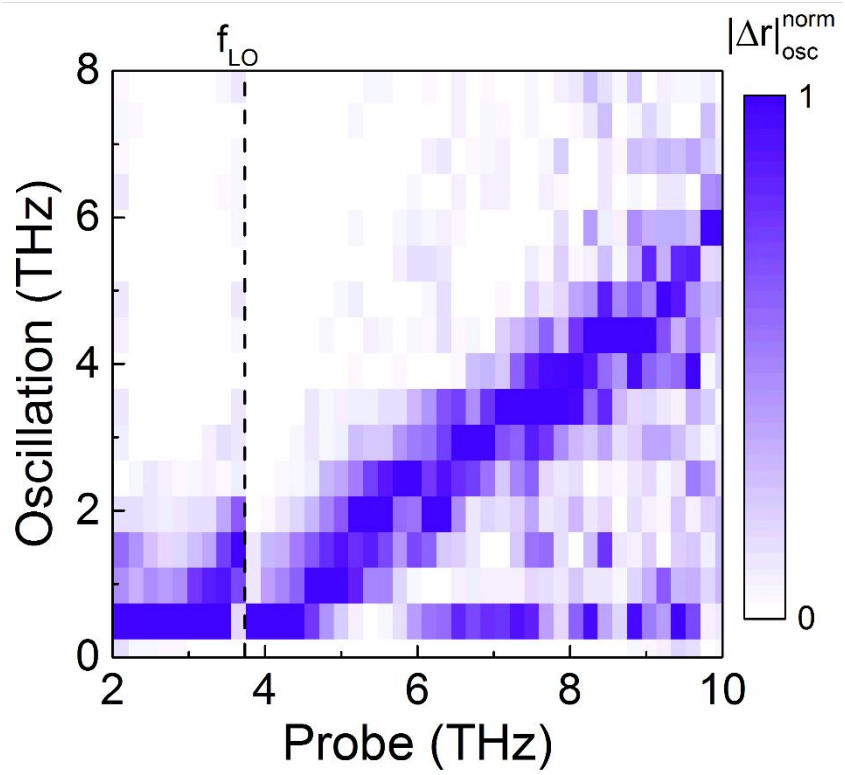

Fig. S6. Fourier domain coherent oscillations of THz reflectivity without slow rise component at ⟨100⟩ facet. Fourier transformation along delay time axis τ, $|\Delta r(\omega, \omega_{osc})|_{osc}^{norm}$, showing a clear onset of a coherent beat between charge motion at ω and ω_{LO}. Information below 0.5 THz in oscillation is restricted by noise.

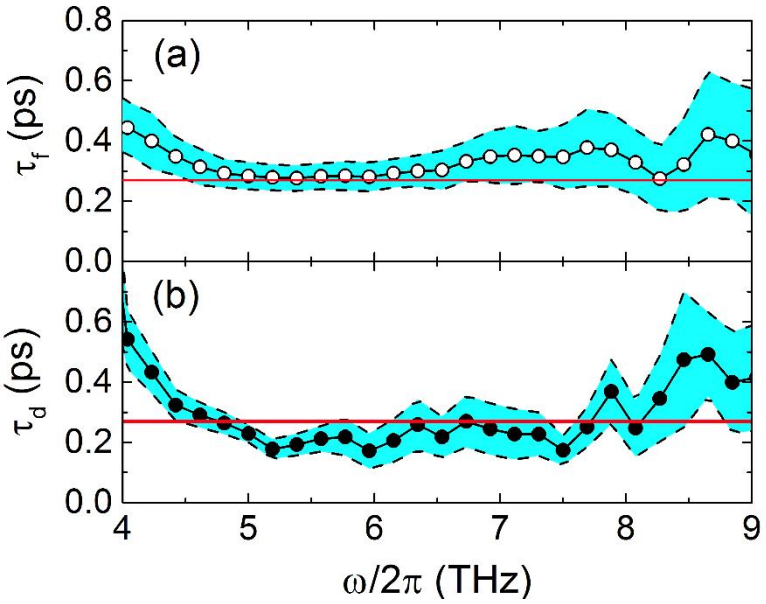

Fig. S7. Time constants at ⟨100⟩ facet. (a) Reflectivity rising time constant τ_r (open circles) with 95 % confidence bounds (shaded area). (b) Quantum beat dephasing time constant τ_d (closed circles) with 95 % confidence bounds (shaded area). The red line marks one phonon period.

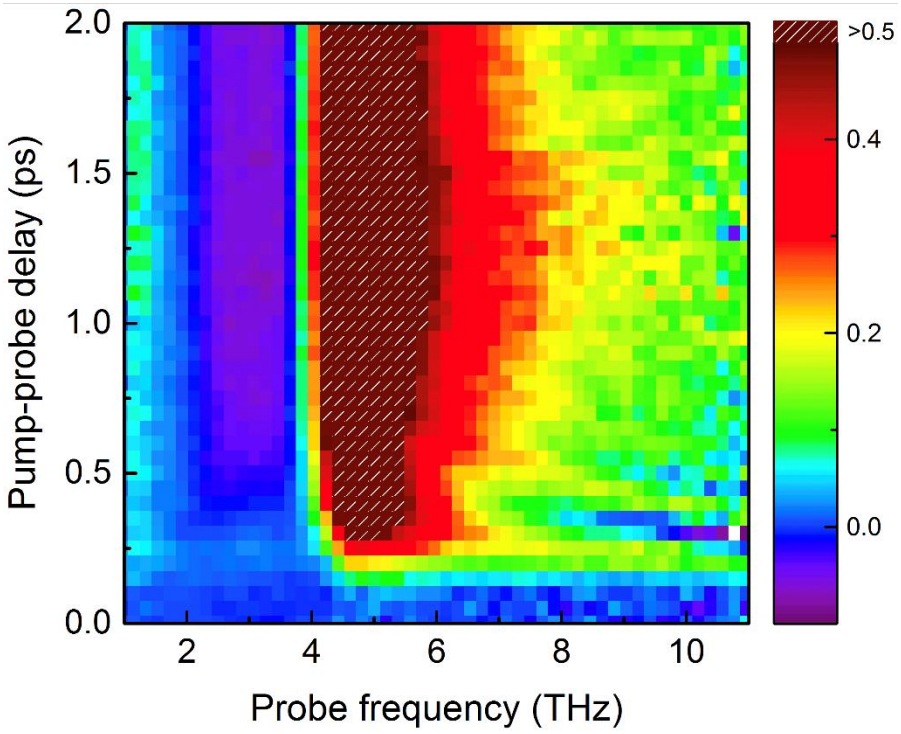

Fig. S8. Amplitude of pump-induced differential THz reflectivity at ⟨111⟩ facet. Two-dimensional time/energy map of amplitude for $\boldsymbol{\Delta r(\omega,\tau)/r_0}$ for the ⟨111⟩ facet, under the same TRTS measurement for the ⟨$11\bar{1}$⟩ facet.

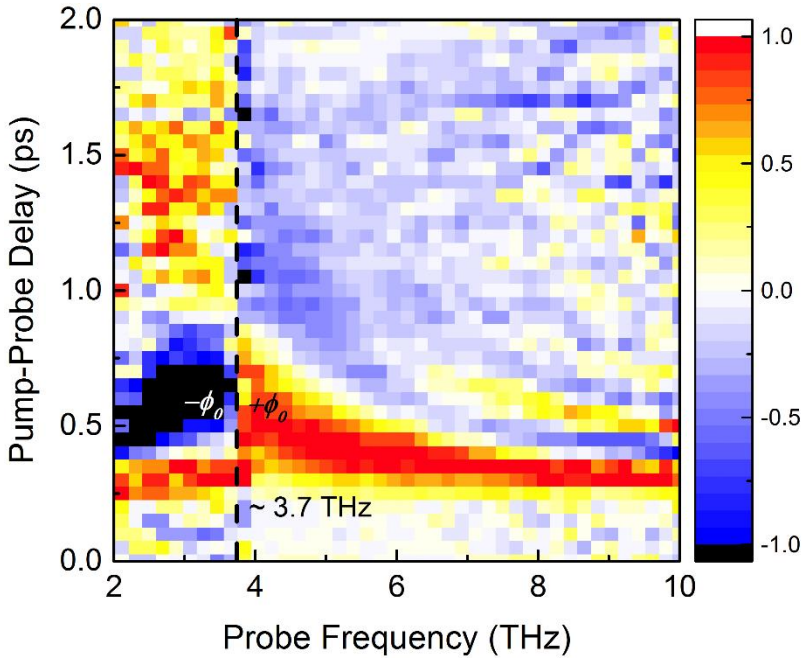

Fig. S9. Time domain coherent oscillations of THz reflectivity without slow rise component at ⟨111⟩ facet. Normalized $|\Delta r(\omega,\tau)|_{osc}^{norm}$ map with slow rise component subtracted. The vertical dash line marks the LO phonon frequency at 3.7 THz where a π phase flip occurs and above which a subsequent frequency chirp is evident.

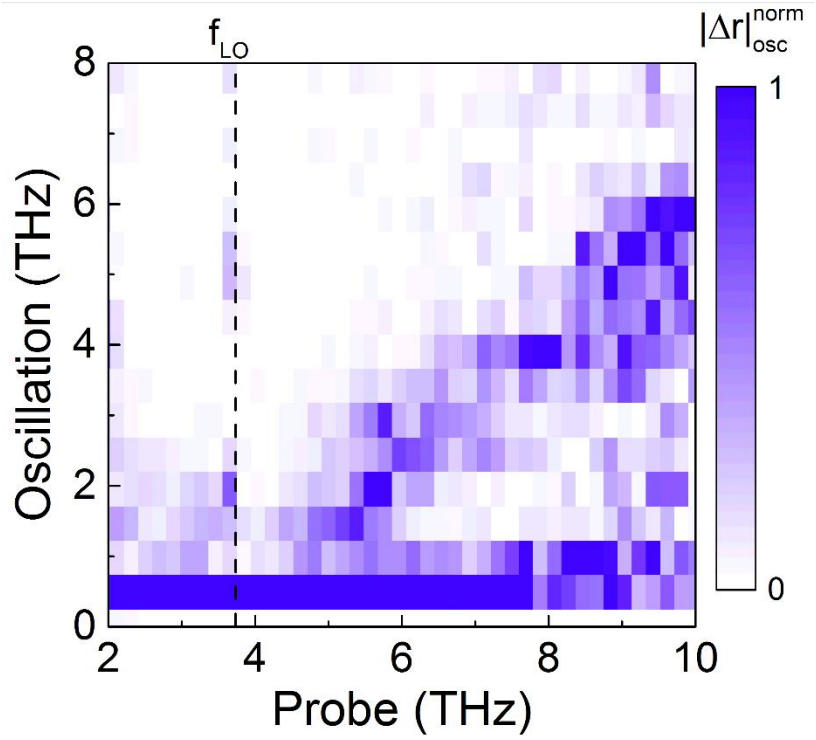

Fig. S10. Fourier domain coherent oscillations of THz reflectivity without slow rise component at ⟨111⟩ facet. Fourier transformation along delay time axis τ, $|\Delta r(\omega, \omega_{osc})|_{osc}^{norm}$, showing a clear onset of a coherent beat between charge motion at ω and ω_{LO}. Information below 0.5 THz in oscillation is restricted by noise.

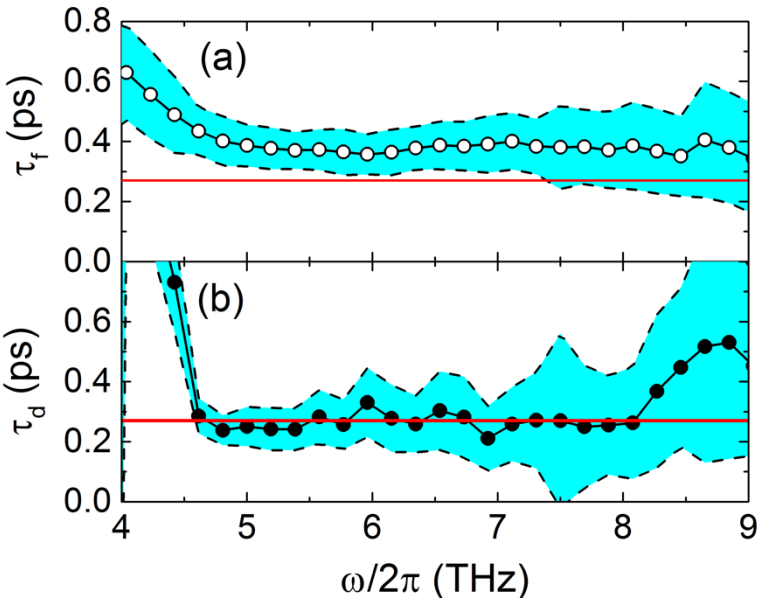

Fig. S11. Time constants at ⟨111⟩ facet. (a)Reflectivity rising time constant τ_r (open circles) with 95 % confidence bounds (shaded area). (b) Quantum beat dephasing time constant τ_d (closed circles) with 95 % confidence bounds (shaded area). The red line marks one phonon period.

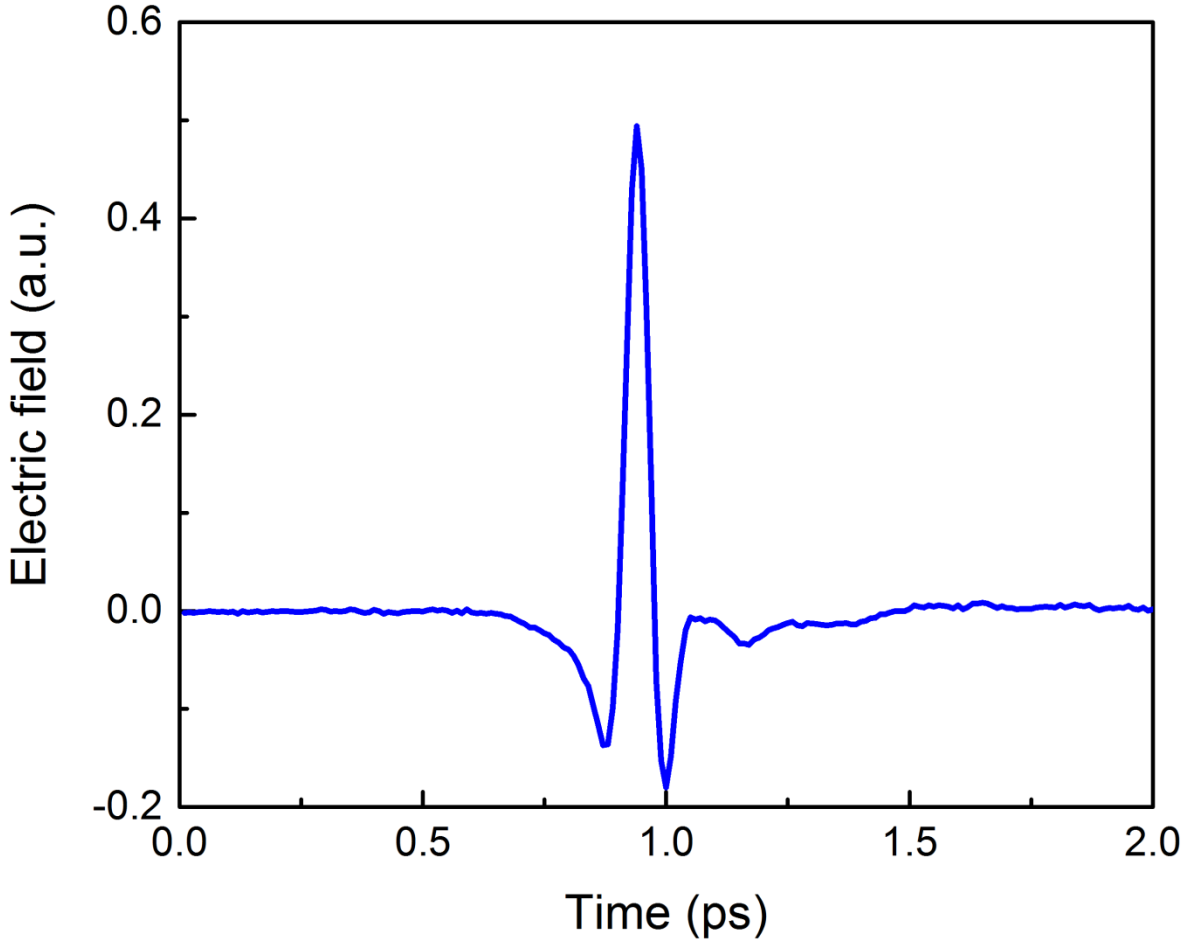

Fig. S12. Electric field in time domain of the reference THz probe pulse. The electric field is directly measured by air-biased-coherent-detection (ABCD), which gives both amplitude and phase information for the THz pulse.

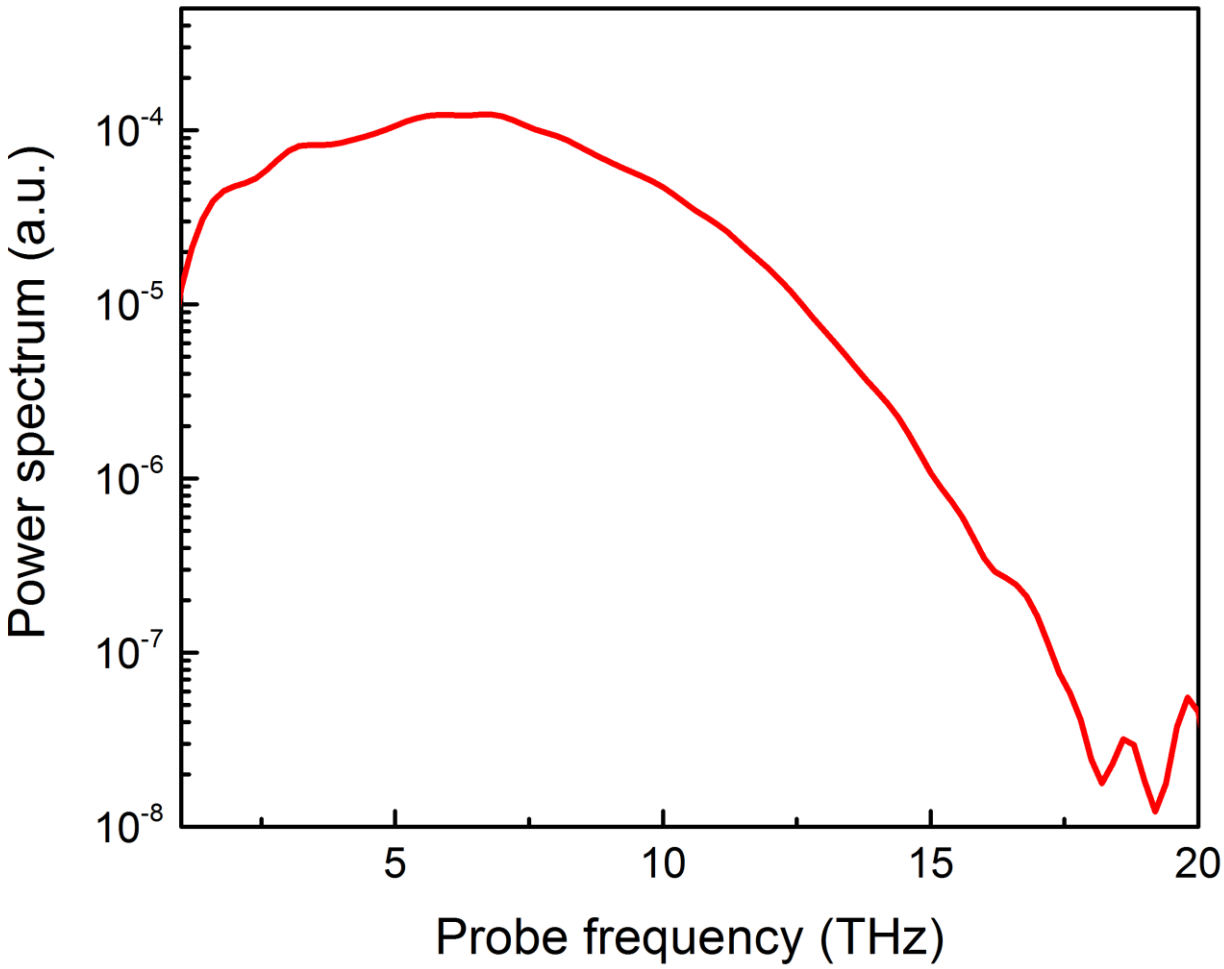

Fig. S13. Power spectrum of the reference THz probe pulse. This is calculated from Fourier transform of the measured THz electric field.

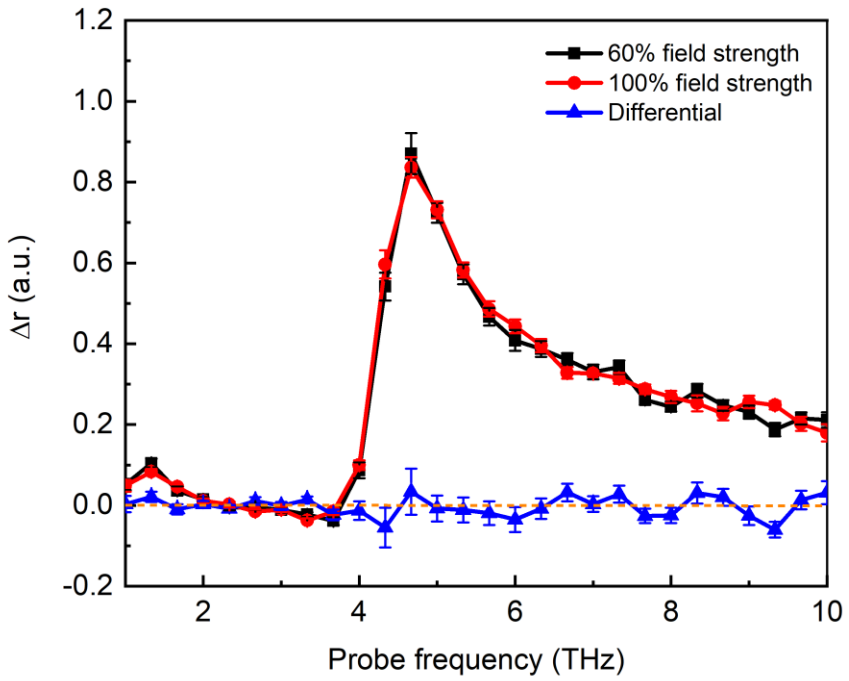

Fig. S14. Pump-induced THz reflectivity change for different probe field strengths. THz differential amplitudes are taken at a pump probe time delay of 250 fs after excitation for the full field strength used in the experiments and the probe field strength reduced by 60%. No variation in the response is observed, verifying linear response. The data corresponds to the red horizontal line cut in the differential reflectivity amplitude map in Fig. 2B of the manuscript (also shown in Fig. 2A.)

Table S1. Parameters describing MAPI dielectric properties. Electron effective mass (m*), LO phonon frequency (ω_{LO}), static and optical dielectric constants (ε_s and ε_∞).

m*	$\hbar\omega_{LO}$	ε_s	ε_∞
$0.23m_0$ (*37*)	15.3meV (*33*)	30 (*31*)	5.5 (*23*)